Analysis of periodically forced nonlinear Hill's oscillator with application to a geared system

C. Padmanabhan[a] and Rajendra Singh[b]
Acoustics and Dynamics Laboratory, Department of Mechanical Engineering, The Ohio State University, Columbus, Ohio 43210-1107

(Received 23 March 1995; accepted for publication 14 September 1995)

Although nonlinear systems subject to combined parametric and external excitations have been examined in some depth, very few of these investigations have addressed the influence of a mean (time-invariant) load on the system response. In particular, the importance of the mean load effect has been highlighted in the study of whirling asymmetric shafts, where significant changes in system response and stability occur under the influence of gravity. The present paper intends to characterize the specific effect of mean load on the dynamic behavior of a Hill's oscillator with a clearance-type nonlinearity while also being subjected to a periodic base displacement excitation. The parametric continuation technique and method of harmonic balance would be used for this purpose. Issues discussed would include the coupling between the mean load and the dynamic response amplitude, interaction between the parametric excitation effect and the clearance nonlinearity, and comparison between time-invariant and time-varying systems. Further, a geared system has been analyzed as a practical application of the nonlinear Hill's equation examined. Earlier studies on gear dynamics have been reexamined to provide improved correlation with prior experimental data; new interpretations for some of the nonlinear phenomena in the experimental data has also been provided based on our study. © *1996 Acoustical Society of America.*

PACS numbers: 43.40.At, 43.25.Ts

INTRODUCTION

Two important class of problems emerge as deviations from the linear differential equations with time-invariant or constant coefficients (LTI). The first group refers to the linear time-varying (LTV) problems, which have been classified as the Hill's or Mathieu's equations, when the time variations of a parameter is sinusoidal or periodic.[1-5] The second group consists of nonlinear differential equations but with time-invariant coefficients (NLTI). The classical literature on differential equations or vibrations treats both time-varying and nonlinear problems separately as stated above.[2-5] Only Den Hartog[1] in his famous book on mechanical vibrations covered both topics under the same broad umbrella of variable elasticity since he believed it to be of major importance in mechanical engineering and related disciplines. McLachlan[2] coined the term nonlinear Hill's equation to describe problems with both time-varying parameters and nonlinear effects; he studied a single-degree-of-freedom oscillator with a time-varying linear stiffness added to a cubic stiffness variation. A number of authors[2-9] have examined similar class of problems but few have considered the effect of a time-invariant or mean load on the system response.

For noncircular shafts, Den Hartog[1] showed that at one-half the critical speed, parametric instability only occurred for horizontal shafts, thus demonstrating the significant effect of gravity in altering system stability. He also established that while instability occurred at critical speed for a vertical shaft the response of the horizontal shaft was stable. Rao[2] expanding on Den Hartog's[1] and Tondl's[3] work obtained an analytical solution for the response of a perfectly balanced horizontal rotor; the influence of gravity caused the system to respond at twice the shaft running frequency and hence any periodic disturbance at twice the running speed could make the system unstable (subharmonic resonance). However, these analyses were limited to linear systems and the effect of an additional external excitation or mean torque was not considered. On the other hand, a number of authors[3-10] have examined the response and stability of time-varying systems including the effect of nonlinearities and/or external excitations, but almost none have considered the influence a time-invariant or mean load has in modifying the stability and response of such systems.

Our interest arises from machinery vibration and acoustics where many real life problems including those with machine elements exhibit periodic parameters (which vary in time or space) and nonlinear characteristics simultaneously. The mechanical model representing them is often under the influence of a *time-invariant or mean force* (torque) and a periodic excitation that is related to the kinematics of the system; similar problems can be found in other applications or disciplines. Consider, for instance, the subject of gear dynamics which essentially represents an application of the nonlinear Hill's equation. It has been identified, for instance, that the periodic variation of the gear tooth meshing stiffness, a consequence of the alternate engagement of m and $m+1$ pairs of teeth, has a significant influence on the geared system's dynamic response. Further, the main source of excitation in a geared system, under *constant torque* loading conditions, is the gear transmission error (which is periodic in time); this error is composed of deviations arising from the

[a]Currently with Copeland Corporation, Sidney, OH 45365.
[b]Corresponding author.

 0001-4966/96/99(1)/324/11/$6.00

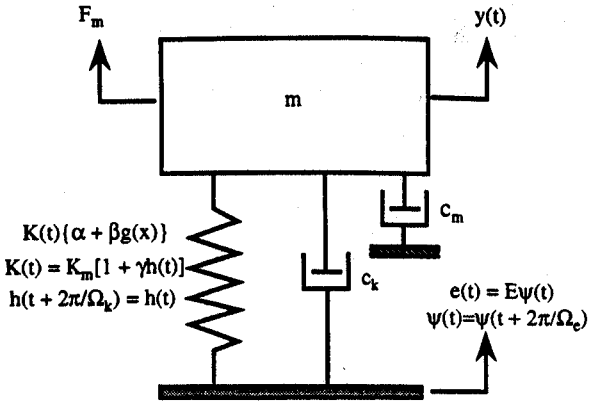

FIG. 1. A single-degree-of-freedom nonlinear Hill's oscillator with base displacement input; the model is under the influence of a mean load F_m. Mass and damping elements are linear and time invariant.

gear tooth deflections under the influence of a mean load, as well as those from manufacturing inaccuracies or modifications. If the dynamic response is sufficiently large in amplitude, nonlinear phenomena such as tooth separation and back collision of teeth can occur, initiated by the presence of gear backlash.

The main objectives of this paper are (1) to investigate the influence of a mean or time-invariant load on the response and stability of a nonlinear Hill's oscillator, and (2) to study the dynamic interaction between the parametric excitation term and the backlash-type nonlinearity. To study the effect of a mean load on system response, we first examine a single-degree-of-freedom (SDOF) oscillator model incorporating periodically time-varying and nonlinear effects. The oscillator model can be thought of as a simplified representation of a geared system and is under the influence of a mean load and a periodic base excitation. Next, we use a three-degree-of-freedom transverse-torsional model of a geared system in order to highlight the interaction between time-varying and nonlinear effects. Some of the simulation results are compared with previously published experimental data to demonstrate validity of the model. Also, this investigation throws light on some of the unexplained phenomena reported in those experiments.

I. PROBLEM FORMULATION

Consider the single-degree-of-freedom (SDOF) mechanical oscillator of Fig. 1 with both time-varying stiffness $K(t)$ and nonlinear elasticity function $f(x)$. The equation of motion is as follows, where the mean force is F_m and the periodic base displacement excitation $e(t)=E\psi(t)$, $\psi(t)=\psi(t+2\pi/\Omega_e)$, Ω_e being the fundamental base excitation frequency:

$$m\ddot{y}+c_k(\dot{y}-\dot{e})+c_m\dot{y}+\alpha K(t)(y(t)-e(t)) + \beta K(t)f(y-e)=F_m, \tag{1}$$

where the elastic constraint force is given by

$$K(t)=K_m[1+\gamma h(t)]. \tag{2}$$

Here, K_m is the mean stiffness, i.e., $K_m=\langle K(t)\rangle_t$. The periodic variation in stiffness is given by $h(t)=h(t+2\pi/\Omega_k)$, where Ω_k is the pumping frequency. Here α, β, and γ are scalar parameters that can be adjusted to suit the problem in hand. On substituting $x(t)=y(t)-e(t)$, one gets the following equation:

$$m\ddot{x}+(c_k+c_m)\dot{x}+\alpha K(t)x(t)+\beta K(t)f(x) =F_m-m\ddot{e}(t)-c_m\dot{e}(t). \tag{3}$$

The nonlinearity, $f(x)$, under consideration is the clearance type and is given by

$$f(x)=\begin{cases} x-b_x, & x\geqslant b_x, \\ 0, & -b_x\leqslant x\leqslant b_x, \\ x+b_x, & x\leqslant -b_x. \end{cases} \tag{4}$$

Equation (3) representing the nonlinear Hill's equation with base excitation is nondimensionalized by choosing $\tau=\Omega N t$, $\Omega_N=\sqrt{K_m/m}$, $p=x/b_c$, $b=b_x/b_c$, $\rho\Omega_N=c_m/\sqrt{K_m m}$, and $2\zeta\Omega_N=(c_k+c_m)/\sqrt{K_m m}$. Further, the stiffness variation and the base displacement input is assumed to be represented by a single harmonic, i.e., $\psi(t)=-h(t)=\cos(\omega\tau)$, with $\omega=\omega_j=\Omega_j/\Omega_N$; $j=e,f$. This leads to the nondimensional equation for base excitation where $f_m=F_m/m\Omega_N^2$:

$$p''+2\zeta p'+\{1-\gamma\cos(\omega\tau)\}f(p) =f_m+\omega^2 E\cos(\omega\tau)+\omega\rho E\sin(\omega\tau). \tag{5}$$

II. DYNAMIC ANALYSIS OF NONLINEAR HILL'S OSCILLATOR

A. Linear time-varying system

Let us solve the above equation for the linear case, i.e., $f(p)=p\forall p$, by using a multiterm harmonic balance scheme.[11] The harmonic balance scheme is chosen over other techniques such as perturbation methods since no limiting assumptions need be made regarding the strength of the parameter γ. It is also fairly straightforward to calculate the effects of higher harmonics in the solution. Further, when the clearance nonlinearity is introduced in later sections conventional perturbation schemes cannot be used as it is a strong nonlinearity; the harmonic balance scheme does not suffer from such a restriction. The procedure assumes a truncated trigonometric expansion for $p(\tau)$:

$$p(\tau)=\frac{p_0}{2}+\sum_{k=1}^{N_t}\{p_{2k-1}\cos(k\omega\tau)+p_{2k}\sin(k\omega\tau)\}. \tag{6}$$

For the linear time-varying (LTV) case ($f(p)=p,\forall p$) one can get the following linear algebraic equation for the harmonic coefficients, p_i, $i=0,\ldots,2N_t$ by substituting Eq. (6) in Eq. (5) and balancing like harmonic terms:

$$\sum_{j=0}^{2N_t}A_{ij}p_j=b_i, \quad i=0,\ldots,2N_t. \tag{7}$$

The nonzero elements of A_{ij} and b_i with $i,j=0,\ldots,2N_t$ are defined below:

$$A_{0,0}=\frac{1}{2}, \quad A_{0,1}=A_{1,0}=-\frac{\gamma}{2}; \tag{8a}$$

$$A_{2k-1,2k-1}=(1-k^2\omega^2), \quad A_{2k-1,2k}=2k\omega\zeta, \quad k=1,\ldots,N_t; \tag{8b}$$

$$A_{2k,2k}=(1-k^2\omega^2), \quad A_{2k,2k-1}=-2k\omega\zeta, \quad k=1,\ldots,N_t; \tag{8c}$$

$$A_{2k-1,2k+1}=A_{2k,2k+2}=A_{2k+1,2k-1}=A_{2k+2,2k}=-\frac{\gamma}{2}, \quad k=1,\ldots,N_t-1; \tag{8d}$$

$$b_0=f_m, \quad b_1=E_1\omega^2, \quad E_1=E. \tag{8e}$$

In Eq. (1) ρ is assumed to be zero. The solution for a one harmonic term ($p(\tau)=p_0/2+p_1\cos(\omega\tau)+p_2\sin(\omega\tau)$) can be given explicitly as

$$p_0=\frac{f_m\{(1-\omega^2)^2+(2\zeta\omega)^2\}+(\gamma/2)\{E_1\omega^2(1-\omega^2)\}}{D}, \tag{9a}$$

$$p_1=\frac{1}{2}\frac{(1-\omega^2)\{f_m\gamma+E_1\omega^2\}}{D}, \tag{9b}$$

$$p_2=\frac{2E_1\zeta\omega^3}{D}, \tag{9c}$$

$$D=\frac{1}{2}\{(1-\omega^2)^2+(2\zeta\omega)^2\}-\left(\frac{\gamma}{2}\right)^2(1-\omega^2). \tag{9d}$$

Equations (9) clearly show that the parametric stiffness coefficient γ introduces a term in the amplitude of the first cosine harmonic, coupling it with the mean load. Unlike a linear time-invariant system (LTI) the steady-state system response is nonzero even in the absence of a forced excitation ($E_1=0$). This is due to the mean load, f_m, in the LTV system acting like an external forcing term. In fact as $\omega\to 0$, these expressions can be approximated as

$$p_0/2\approx 2f_m/(2-\gamma^2), \quad p_1\approx 2f_m\gamma/(2-\gamma^2), \quad p_2\approx 0. \tag{10}$$

Consider the case when the stiffness variation and the base displacement excitation are periodic and contain more harmonics, for instance, as shown in Fig. 2. Asymptotically the peak–peak amplitude of the response, p, still follows Eq. (9) as seen in Fig. 3(a) where $f_m=0.10$ and $\gamma=0.20$ and in Fig. 3(b), where $f_m=0.10$ and $\gamma=0.38$. These figures also show a comparison between the system responses, obtained by a multiterm harmonic balance scheme numerically, without and with the presence of a base displacement excitation. The forced excitation causes significant effect mainly at the higher frequencies and has little effect at frequencies below $\omega\approx 0.15$. Figure 4 shows the variation with ω, of amplitudes of the first three harmonics of p corresponding to $f_m=0.10$ and $\gamma=0.38$. Observe that even in the absence of the excitation, there are parametric resonances at $\omega=1,\frac{1}{2},\frac{1}{3},\frac{1}{4},\ldots$, etc. The system can exhibit instability at these parametric resonances

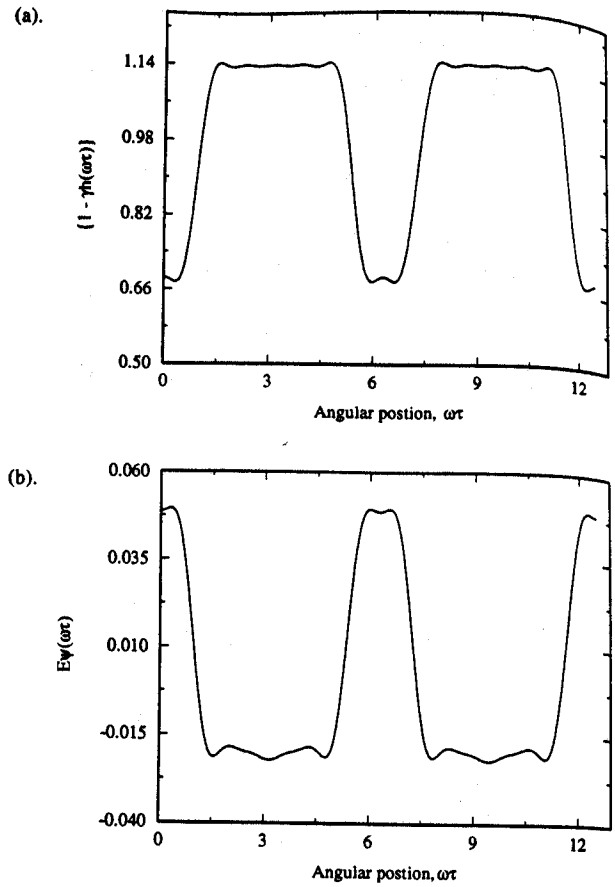

FIG. 2. Periodic time profiles of stiffness and base displacement excitation, (a) stiffness variation and (b) displacement excitation variation.

and at subharmonic resonances like $\omega=2$. Figure 5 shows a plot of the instability regimes around $\omega=1$ and $\omega=\frac{1}{2}$ for various damping levels. Such plots are usually referred to as the Strutt diagrams.[3–5] In order to demonstrate differences between an LTV and an LTI system, we plot the coincidence and quadrature of the second harmonic of $p(\tau)$. As seen from Fig. 6, one can see that the LTV system behaves like a MDOF linear time-invariant system due to the presence of the parametric resonances. In each of the regimes between the resonances, the co-quad plot looks similar to a single-degree-of-freedom LTI system.

B. Nonlinear time-varying system

Now we include the effect of backlash, thus making the system nonlinear. The system responses shown in this and later sections are obtained by using the parametric continuation scheme[12–14] which is outlined briefly below.

The parametric continuation method is based on the shooting method, which has been applied classically to solve boundary value problems. Since periodic solutions and their stability are of interest in our case, the initial value problem is transformed to a boundary value problem with periodic end conditions. The shooting procedure[12–14] is applied iteratively, using direct numerical integration from $\tau=0$ to $\tau=\tau_0$, until $p(0)=p(\tau_0)$, where $\tau_0=2\pi m/\omega$, m being an integer; $m=1$, for instance, would yield solutions which have the

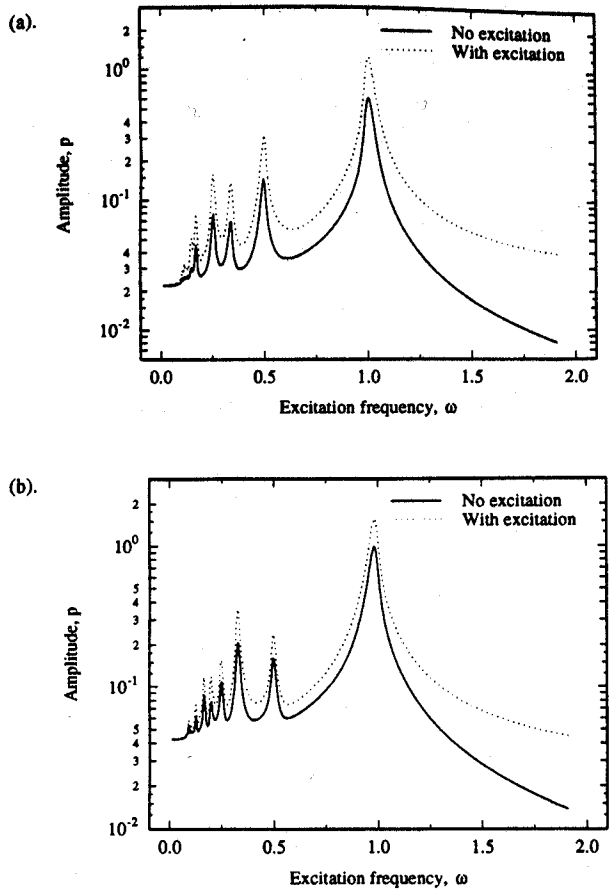

FIG. 3. The frequency response of an LTV system subject to base excitation, (a) with $f_m=0.10$, $\gamma=0.20$ and (b) with $f_m=0.10$, $\gamma=0.38$.

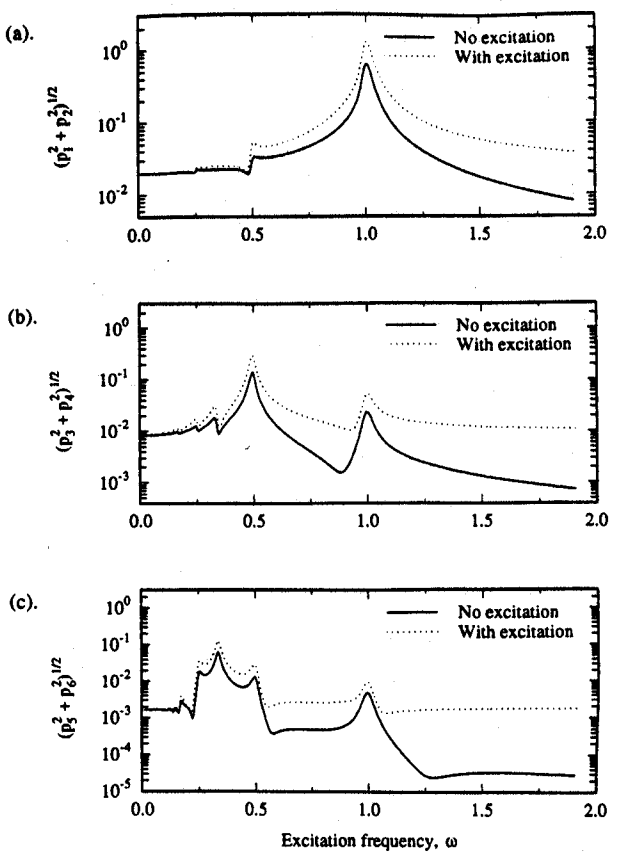

FIG. 4. The amplitude response of the first three harmonics of the LTV system subject to base excitation (a) first harmonic, (b) second harmonic, and (c) third harmonic.

same fundamental period (called period 1 or P1) as the forcing function while $m=2$ would yield subharmonic solutions (termed period 2 or P2), whose fundamental frequency is one-half of the forcing frequency. The periodicity boundary condition for say $m=1$ would require the following nonlinear equation be satisfied:

$$G_i(\eta_i)=\Phi_i(\eta_i)-\eta_i=0, \quad \Phi_i(\eta_i)=q_i(\tau_0), \quad \eta_i=q_i(0), \quad i=1,2, \tag{11}$$

where $q_1=p$, $q_2=p'$. This equation is solved using a Newton–Raphson technique which requires the Jacobian as shown below:

$$J_{ij}=\frac{\partial G_i}{\partial \eta_j}=\left\{\frac{\partial \Phi_i}{\partial \eta_j}-\delta_{ij}\right\}, \quad i,j=1,2, \quad \delta_{ij}=\begin{cases}0, & i\neq j,\\ 1, & i=j.\end{cases} \tag{12}$$

In order to solve for the Jacobian elements as well as to examine the stability of the *fixed point* solution $p_i(0)$ to Eq. (11), variational equations shown below, with $\mu_{ij}=\partial q_i/\partial p_j(0)$, $i,j=1,2$, are obtained by a perturbation of the governing second-order differential equation, Eq. (5), with respect to p:

$$\begin{bmatrix}\mu'_{11} & \mu'_{12}\\ \mu'_{21} & \mu'_{22}\end{bmatrix}=\begin{bmatrix}0 & 1\\ -\dfrac{\partial f(p)}{\partial p}(1-\gamma h(\tau)) & -2\zeta\end{bmatrix}\times\begin{bmatrix}\mu_{11} & \mu_{12}\\ \mu_{21} & \mu_{22}\end{bmatrix}. \tag{13}$$

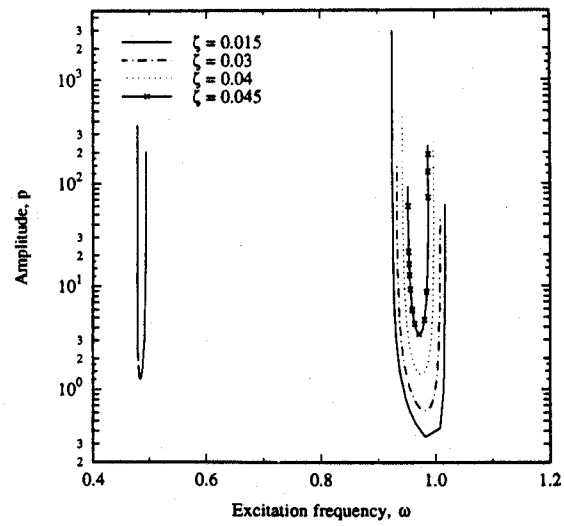

FIG. 5. Instability regimes of an LTV system with base excitation for various damping values.

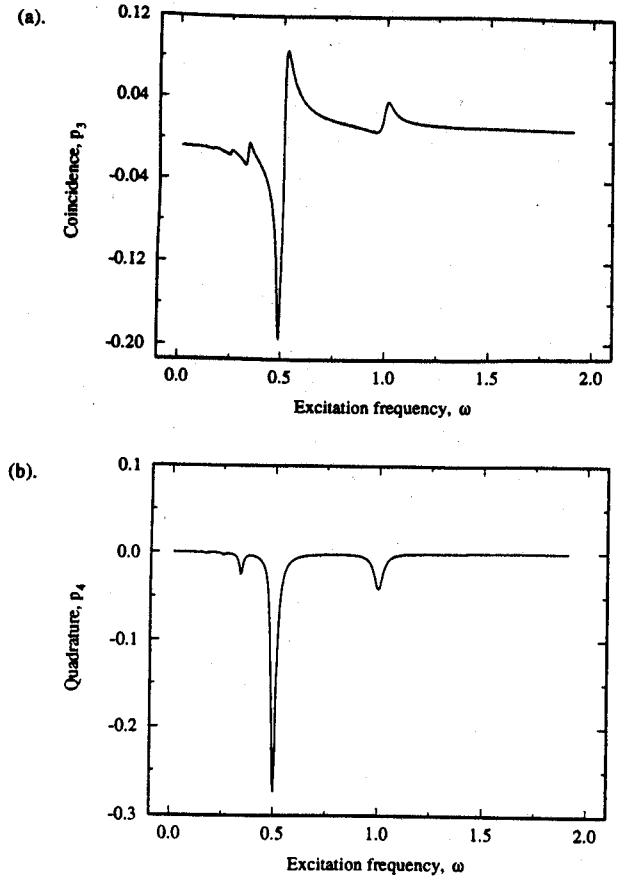

FIG. 6. Co-quad plot for the second harmonic of the response shown in Fig. 4, (a) coincidence, p_3, and (b) quadrature, p_4.

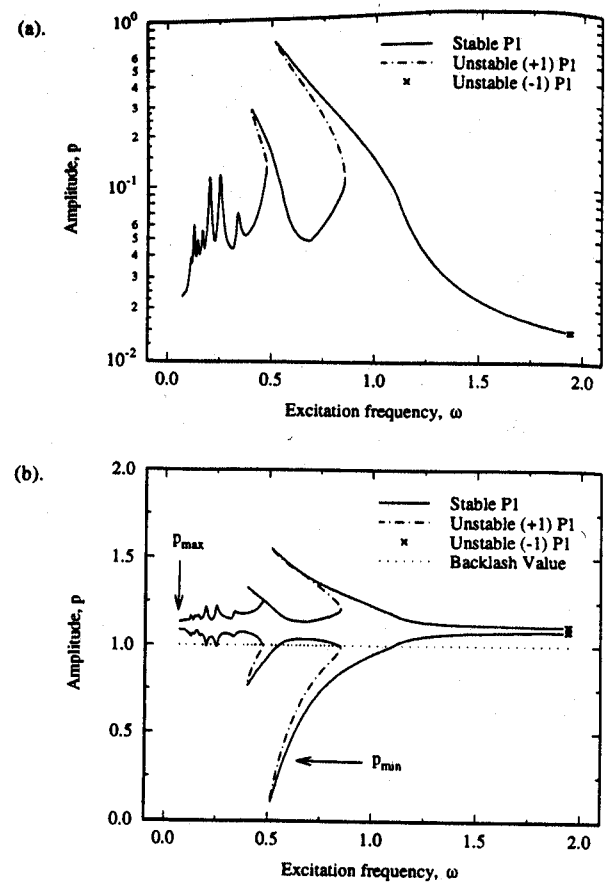

FIG. 7. Frequency response of the nonlinear Hill's oscillator corresponding to Fig. 2, (a) total response and (b) impact transitions.

These equations are then numerically integrated from $\tau=0$ to $\tau=m\tau_0$ along with Eq. (5) to yield the Jacobian matrix:

$$\mathbf{J}=\begin{bmatrix} \mu_{11}(m\tau_0)-1 & \mu_{12}(m\tau_0) \\ \mu_{21}(m\tau_0) & \mu_{22}(m\tau_0)-1 \end{bmatrix}. \tag{14}$$

The eigenvalues λ_i $(i=1,2)$ of the Jacobian matrix, $\mathbf{J}$, thus obtained, determine the stability of the fixed point. If $|\lambda_i|<1$ the fixed point and the hence the system response is stable. Stability is usually lost in three different ways: $\lambda_i=1$, called the *saddle-node bifurcation*; $\lambda_i=-1$, called period-doubling or *pitchfork bifurcation*; a pair of complex conjugates with $|\lambda_i|=1$, called *secondary Hopf bifurcation*.

To overcome the singularities caused by the saddle-node bifurcation for $m=1$ and pitchfork bifurcation for $m=2$, additional parametric equations, shown below for ω as a parameter where $\sigma_1=\partial q_1/\partial\omega$, $\sigma_2=\partial q_2/\partial\omega$, are obtained from a perturbation of the governing equation with respect to ω:

$$\begin{Bmatrix} \sigma_1' \\ \sigma_2' \end{Bmatrix}=\begin{bmatrix} 0 & 1 \\ -[1-\gamma h(\tau)]\dfrac{\partial f(p)}{\partial p} & -2\zeta \end{bmatrix}\begin{Bmatrix} \sigma_1 \\ \sigma_2 \end{Bmatrix} + \begin{Bmatrix} 0 \\ -\omega f_p \sin(\omega\tau) \end{Bmatrix}. \tag{15}$$

The above equations are numerically integrated along with the variational and governing differential equations from $\tau=0$ to $\tau=m\tau_0$. With this procedure then, a complete frequency response or a variation of the response with a parameter like f_m for a fixed ω (including the *unstable* solutions) can be obtained quite efficiently.

Figure 7 shows the frequency response of the SDOF system (obtained using the parametric continuation technique described above), corresponding to a stiffness variation and base displacement shown in Fig. 2. The damping value $2\zeta=0.06$ and the mean load $f_m=0.10$. As can be seen from Fig. 7(a), the primary and secondary parametric resonances show a softening effect. This can be explained from Fig. 7(b) which shows a plot of the maximum and minimum values of $p(\tau)$. The system undergoes a transition from no-impact to single-sided impact at around $\omega=1.12$ as the excitation frequency is reduced and again near $\omega=0.35$ as the frequency is increased. The loss of contact implies a reduction in effective stiffness leading to a softening effect. Next, the level of the excitation is increased and Fig. 8 shows the resulting frequency response. Figure 8(a) shows a comparison of the solution obtained by the continuation method and a multiterm harmonic balance method. The harmonic balance scheme needed about 10–15 harmonics to obtain this excellent match. In Fig. 8(b) the $\frac{1}{2}$ order subharmonic solution (P2) branch is shown along with the regular P1 solutions. For a

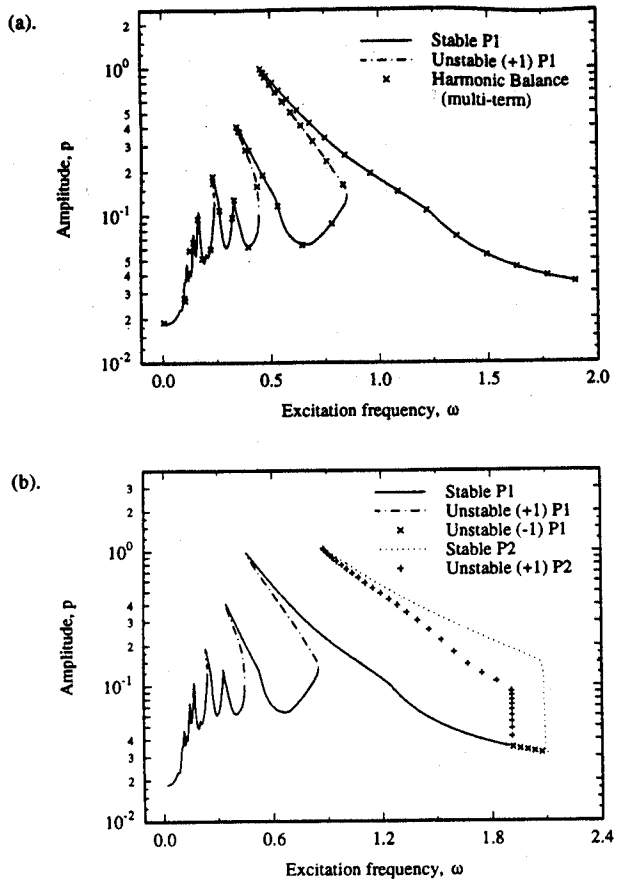

FIG. 8. Frequency response of the nonlinear Hill's oscillator, (a) comparison between continuation and multiterm harmonic balance scheme, (b) the subharmonic P2 loop of the frequency response.

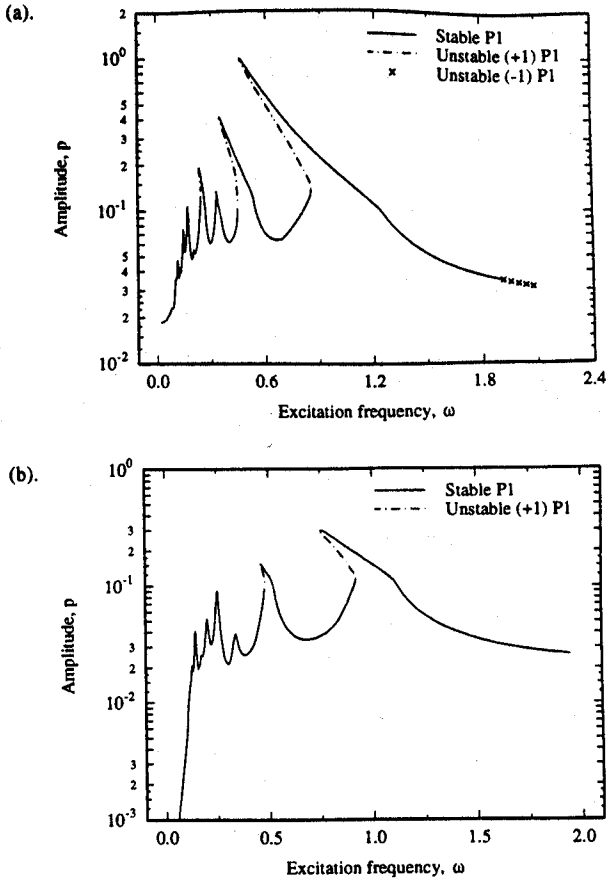

FIG. 9. Comparison of the frequency response between (a) NLTV system (γ=0.20) and (b) NLTI system (γ=0).

wide range of frequencies there are coexisting stable P1 and P2 solutions. In order to quantify the effect of the parametric term on the nonlinear system response, a comparison is made between the response of the nonlinear SDOF model with time-varying stiffness and with constant stiffness (γ=0). Figure 9(a) corresponds to the time-varying stiffness case and Fig. 9(b) refers to the time-invariant stiffness case. One can clearly observe that the effect of the parametric term is to enhance the nonlinear effects leading to higher peak values. Further, at low frequencies the presence of the stiffness variation leads to a nonzero response, while for the constant stiffness case the amplitude asymptotes to zero. The presence of the parametric term causes a subharmonic resonance around ω=2.0 [see Fig. 8(b)], which disappears in Fig. 9(b).

Finally we take a look at the co-quad plots of the NLTV case. Figure 10 shows the co-quad curves for the second harmonic of the response, $p(\tau)$, with the system parameters similar to Fig. 8. It is apparent that at very low or very high frequencies, the system tends to behave like the LTV system. The presence of the backlash distorts the curve leading to multivalued solutions in the range $0.35 \leq \omega \leq 0.85$. Also it is clear from these figures that at lower frequencies the system response is dominated by the higher harmonics.

In summary then, the parametric term introduces three major effects to the system response. First, it introduces additional parametric resonances (both super- and subharmonic types). Second, it produces an interesting coupling effect, i.e., the response amplitude is proportional to the mean load. Finally in the presence of time-varying stiffness tends to enhance the effect of the clearance nonlinearity.

III. APPLICATION OF NONLINEAR HILL'S EQUATION TO A GEARED SYSTEM

In this section we reexamine some of the issues discussed in the previous section in the context of a geared system, which represents a practical application of the nonlinear Hill's equation. Özgüven and Houser[15] provide a detailed review of various gear dynamic models, and what follows is a summary of relevant literature. Hortel[16] was among the first to develop a multi-degree-of-freedom (MDOF) model for a gear pair using Lagrangian mechanics. The model included the parametric excitation effect due to the periodic variation of gear tooth rigidity, as well as the effect of transmission error excitation. His analysis, based on a Fourier series expansion, was, however, for the linear case (although time varying). Munro[17] carried out extensive experiments on a spur gear pair of unity ratio, for a variety of mean torque conditions. In his investigation, he observed the occurrence of subharmonic and quasiperiodic solutions, even under design load conditions (a heavily loaded situation). His analysis, based on the Mathieu's equation,[3-5] predicted the possible presence of a subharmonic resonance. However, the

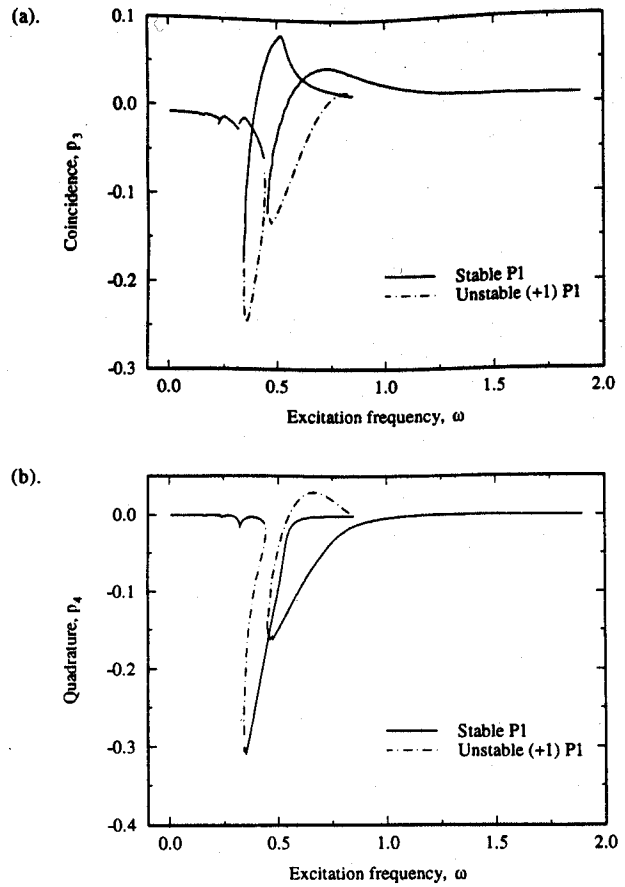

FIG. 10. Co-quad plot for the second harmonic of the response of the nonlinear Hill's equation with (a) coincidence, p_3, and (b) quadrature, p_4.

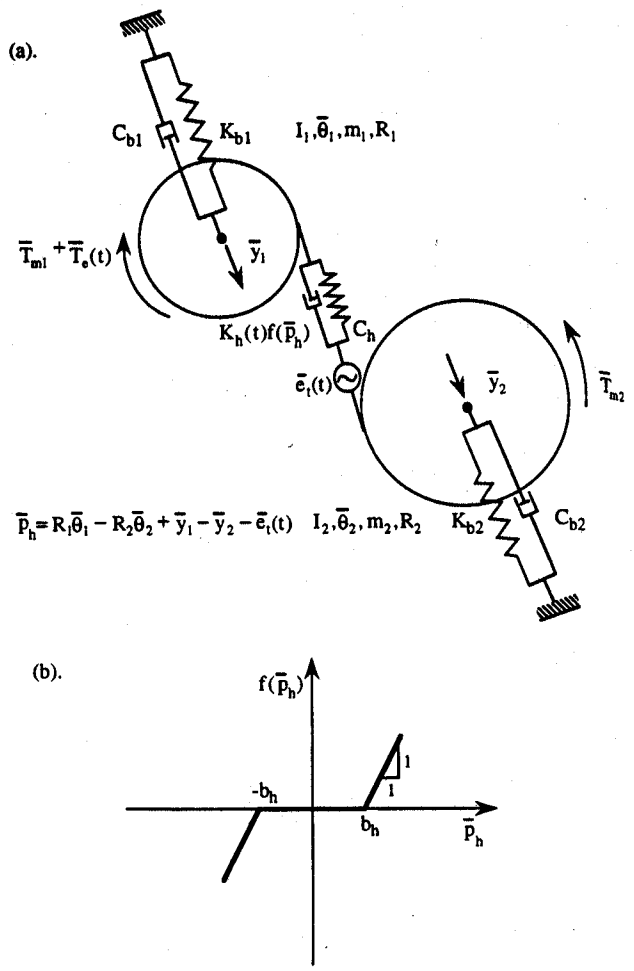

FIG. 11. The coupled transverse-torsional model of a gear pair, (a) the schematic of the system and (b) the nonlinear function representing gear backlash.

system parameters were such that there was a near 1:2 ratio, over most loading conditions, between the two transverse-torsional natural frequencies. Munro observed quasiperiodic, beating-type phenomena in his experiments, but could not explain these by his simple analysis.

Kücükay[18] used an eight-degree-of-freedom model based on multibody dynamics, which included trapezoidal mesh stiffness variation, transmission error excitation and gear backlash, and bearing flexibilities. The stability of periodic solutions near the combination and parametric resonances was determined by numerical integration, based on the Floquet theory. His conclusion was that for both spur and helical gears, instabilities can probably occur at the double-tooth eigenfrequency. Kahraman and Singh[19] have identified the possibility of subharmonic, quasiperiodic, or chaotic solutions based on a three-degree-of-freedom model of the gear pair; they did not, however, attempt to quantify the parameter regimes where such solutions were more likely. In the following section the model developed by Kahraman and Singh[19] will be used to validate and explain some of the experimental phenomena (previously unexplained) reported in the literature.[17,20]

A. Governing equations

The governing equations for a three-degree-of-freedom model of the gear pair shown in Fig. 11 is shown below; refer to Kahraman and Singh[19] for more details:

$$[\mathbf{M}]\{\ddot{\mathbf{z}}\}+[\mathbf{C}]\{\dot{\mathbf{z}}\}+[\mathbf{K}(t)]\{\mathbf{g}(\mathbf{z})\}=\{\mathbf{E}_m\}+\{\mathbf{E}_e(t)\}; \quad (16)$$

$$\mathbf{z}=[\bar{y}_1 \quad \bar{y}_2 \quad \bar{p}_h]^T; \quad \mathbf{g}(\mathbf{z})=[\bar{y}_1 \quad \bar{y}_2 \quad f(\bar{p}_h)]^T; \quad (17)$$

$$[\mathbf{M}]=\begin{bmatrix} m_1 & 0 & 0 \\ 0 & m_2 & 0 \\ -m_g & m_g & m_g \end{bmatrix}, \quad (18)$$

$$[\mathbf{C}]=\begin{bmatrix} C_{b1} & 0 & C_h \\ 0 & C_{b2} & -C_h \\ 0 & 0 & C_h \end{bmatrix};$$

$$[\mathbf{K}(t)]=\begin{bmatrix} K_{b1} & 0 & K_h(t) \\ 0 & K_{b2} & -K_h(t) \\ 0 & 0 & K_h(t) \end{bmatrix},$$

$$\{\mathbf{E}_m\}=\begin{Bmatrix} \bar{F}_{b1} \\ \bar{F}_{b2} \\ \dfrac{\bar{T}_{m1}}{R_1} \end{Bmatrix}, \quad (19)$$

TABLE I. Simulation parameters extracted from experimental data of Munro[17] and Kubo.[20]

Reference	Stiffness (nondimensional)	Damping (nondimensional)	Mean load, F_m	Transmission error, e_t
Kubo[20] no gear error	$\begin{bmatrix} 12.5 & 0 & 0.245 \\ 0 & 13.5 & -0.245 \\ 12.5 & -13.5 & 1.49 \end{bmatrix}$	$\begin{bmatrix} 0.053 & 0 & 0.007 \\ 0 & 0.052 & -0.007 \\ 0.024 & -0.021 & 0.08 \end{bmatrix}$	0.135	0.04
Kubo[20] with gear error	$\begin{bmatrix} 12.5 & 0 & 0.245 \\ 0 & 13.5 & -0.245 \\ 12.5 & -13.5 & 1.49 \end{bmatrix}$	$\begin{bmatrix} 0.053 & 0 & 0.007 \\ 0 & 0.052 & -0.007 \\ 0.024 & -0.021 & 0.08 \end{bmatrix}$	0.135	0.012
Munro[17] design load	$\begin{bmatrix} 0.94 & 0 & 0.245 \\ 0 & 0.94 & -0.245 \\ 0.94 & -0.94 & 1.49 \end{bmatrix}$	$\begin{bmatrix} 0.047 & 0 & 0.0 \\ 0 & 0.047 & -0.0 \\ 0.03 & -0.03 & 0.09 \end{bmatrix}$	0.183	0.006
Munro[17] half-design load	$\begin{bmatrix} 0.83 & 0 & 0.245 \\ 0 & 0.83 & -0.245 \\ 0.83 & -0.83 & 1.49 \end{bmatrix}$	$\begin{bmatrix} 0.04 & 0 & 0.0 \\ 0 & 0.04 & -0.0 \\ 0.027 & -0.027 & 0.09 \end{bmatrix}$	0.105	0.03

$$\{\mathbf{E}_e(t)\}=\begin{Bmatrix} 0 \\ 0 \\ -m_g\ddot{e}_t(t)+\lambda\dfrac{\bar{T}_e(t)}{R_1} \end{Bmatrix};$$

$$f(\bar{p}_h)=\begin{cases} \bar{p}_h-b_h, & \bar{p}_h>b_h, \\ 0, & -b_h\leq\bar{p}_h\leq b_h, \\ \bar{p}_h+b_h, & -b_h>\bar{p}_h; \end{cases} \tag{20}$$

$$1/m_g=(R_1^2/I_1)+(R_2^2/I_2); \quad \lambda=\{1+(I_1R_2^2/I_2R_1^2)\}^{-1},$$
$$\bar{p}_h=R_1\bar{\theta}_1-R_2\bar{\theta}_2+\bar{y}_1-\bar{y}_2-\bar{e}_t. \tag{21}$$

The time-varying mesh stiffness is periodic, with a fundamental time period, $t_h=2\pi/\bar{\Omega}_h$; $\bar{\Omega}_h=N_p\bar{\Omega}_s$, where N_p is the number of pinion teeth and $\bar{\Omega}_s$ is the shaft rotation frequency in rad/s. The transmission error, $e_t(t)$, is also periodic with the same fundamental time period as the mesh stiffness variation, provided no misalignment or run-out errors are considered. Equation (16) is nondimensionalized both in time and space by defining $\tau=\Omega_N t$ and dividing all the variables with respect to the backlash b_h. This yields the following equation:

$$\begin{bmatrix} 1 & 0 & 0 \\ 0 & 1 & 0 \\ -1 & 1 & 1 \end{bmatrix}\begin{Bmatrix} y_1'' \\ y_2'' \\ p_h'' \end{Bmatrix}+\begin{bmatrix} \zeta_{11} & 0 & \zeta_{13} \\ 0 & \zeta_{22} & -\zeta_{23} \\ 0 & 0 & \zeta_{33} \end{bmatrix}\begin{Bmatrix} y_1' \\ y_2' \\ p_h' \end{Bmatrix}$$
$$+\begin{bmatrix} \kappa_{11} & 0 & \kappa_{13}(\tau;\tau_m) \\ 0 & \kappa_{22} & -\kappa_{23}(\tau;\tau_m) \\ 0 & 0 & \kappa_{33}(\tau;\tau_m) \end{bmatrix}\begin{Bmatrix} y_1 \\ y_2 \\ f(p) \end{Bmatrix}$$
$$=\begin{Bmatrix} F_{b1} \\ F_{b2} \\ F_m \end{Bmatrix}+\begin{Bmatrix} 0 \\ 0 \\ -e_t''(\tau;\tau_m,\tau_s)+F_e(\tau;\tau_s) \end{Bmatrix}; \tag{22}$$

$$\zeta_{ii}=\frac{C_{bi}}{m_i\Omega_N}, \quad \zeta_{i3}=\frac{C_m}{m_i\Omega_N}, \quad \zeta_{33}=\frac{C_m}{m_g\Omega_N}, \quad i=1,2; \tag{23}$$

$$\kappa_{ii}=\frac{K_{bi}}{m_i\Omega_N^2}, \quad \kappa_{i3}(\tau)=\frac{K_m(\tau)}{m_i\Omega_N^2},$$
$$\kappa_{33}(\tau)=\frac{K_m(\tau)}{m_g\Omega_N^2}, \quad i=1,2; \tag{24}$$

$$F_{bi}=\frac{\bar{F}_{bi}}{m_i\Omega_N^2b_c}, \quad F_m=\frac{\bar{T}_{m1}}{R_1m_g\Omega_N^2b_c},$$
$$F_e(\tau)=\lambda\frac{\bar{T}_e(t)}{R_1m_g\Omega_N^2b_c}, \quad i=1,2. \tag{25}$$

B. Interpretation of prior experimental data

The equations representing the dynamics of the three-degree-of-freedom model[18] developed in the previous section is now used to validate prior published results based on the experimental testing of spur gears.[17,20] Table I lists the parameters used in this study. These parameters correspond to Munro's experimental setup for various loading conditions[17] and Kubo's experimental apparatus for testing spur gears with and without gear errors.[20] It can be seen that the parameters for Munro's rig[17] lead to a near 1:2 relationship between the first and second transverse-torsional resonances over most loading conditions. The variation of stiffness and transmission error were estimated based on the data provided.[20] For Kubo's setup the bearings and shafts are much stiffer leading to a very high second transverse-torsional resonance. Again, based on the information about the gears, the gear errors and stiffness transmission error profiles have been estimated from Ref. 20. Figure 12 shows the complete response of the dynamic transmission error $p_h(\tau)$ and $y_2(\tau)$ for Kubo's parameters with and without gear errors. The damping matrix was calculated based on an assumption of 3%–5% modal damping. This system exhibits a number of superharmonic resonances. There is also the softening effect near the first linear transverse-torsional resonance. However, the system does not exhibit subharmonic or

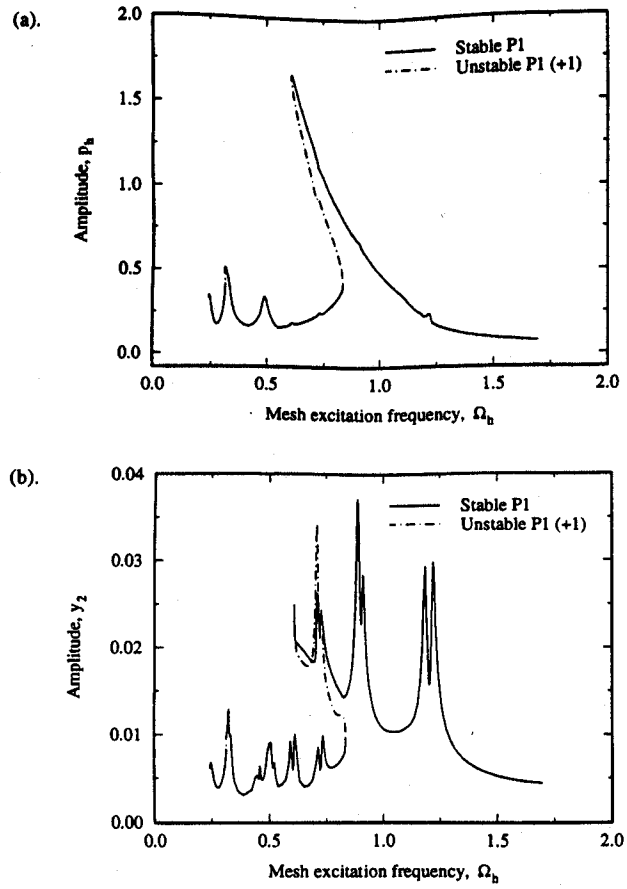

FIG. 12. Simulation results for Kubo's experimental system:[20] (a) dynamic transmission error, p_h, and (b) bearing displacement, y_2; see Table I for parameters used.

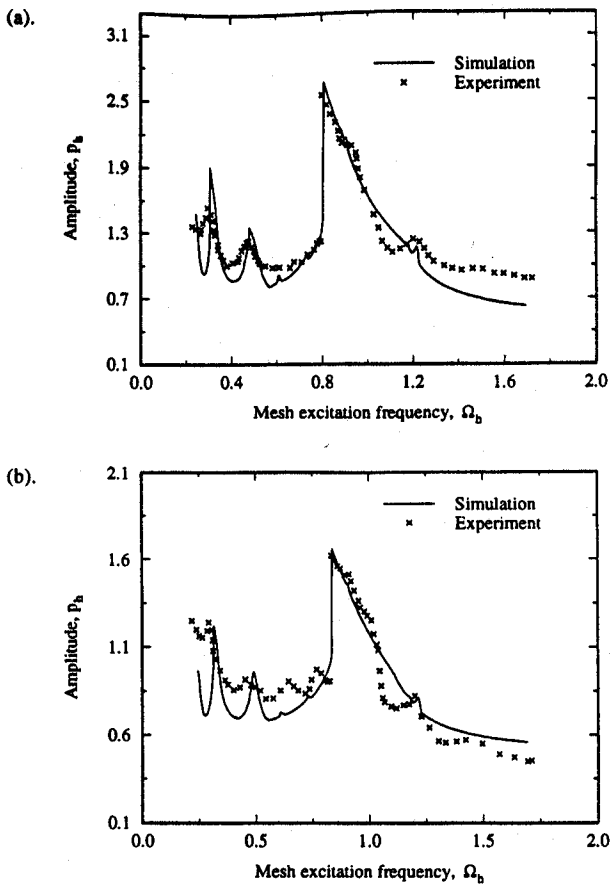

FIG. 13. Comparison of simulation and experimental results for Kubo's rig:[20] (a) no gear error and (b) with gear error; see Table I for parameters used.

nonperiodic solutions. Figure 13 shows the comparison between simulation and Kubo's experimental data for the two cases (with and without gear errors). The simulation results correspond to the stable portions of Fig. 12, which have been scaled to relate to dynamic factor plots of Kubo.[20] Notice the excellent correlation between predicted and measured resonant peaks as well as a reasonable match in predicting amplitudes. Kahraman and Singh[19] had used a heavily damped (ζ_{33}=0.20) SDOF model to correlate this particular experiment data. But their SDOF model could not explain the peak near $\Omega_h \approx 1.2$. This is a superharmonic resonance peak (order 3) of the second transverse-torsional mode and is predicted quite well by the full three-degree-of-freedom model. Also, the damping levels used in the present simulation model were much lower than that used by Kahraman and Singh.[19] Munro's rig[17] leads to more dynamic interactions than those corresponding to Kubo's case.[20] The gears tested were designed to have minimum transmission error at design load. In order to compare the experimental results with those of the simulation, only two loads were picked—one being the design load and the other is half the design load, where a bigger effect of the nonlinearity on the system dynamics is anticipated. Figures 14 and 15 show the complete response obtained for the design and half-design load conditions, respectively. Notice that in both cases the system exhibits stable subharmonic solutions (type P2) around the second linear transverse-torsional resonance. This prediction is in agreement with the experimental results where P2 solutions occur around the second resonance. Figure 16 shows the comparison between experiment and the stable parts of the simulation results of Figs. 14 and 15. For the half-design load case, several regimes exist where stable quasiperiodic solutions can occur. Again this prediction by the present simulation model is in close agreement with the effects reported by Munro.[17] This effect can be possibly due to the 1:2 internal resonance. In a multi-degree-of-freedom system, an internal resonance occurs when any two linear natural frequencies of the system have an almost integer ratio, i.e., $\omega_k \approx j\omega_l = j\omega_l + \epsilon, j$ being an integer. This may lead to an exchange of energy between the two corresponding modes modulated by the difference in the frequencies, ϵ, causing quasiperiodic or beating-type response.

IV. CONCLUSION

In this paper, various issues related to the nonlinear Hill's equation have been highlighted. The mean load has been shown to have a significant influence when the system has time-varying parameters. A coupling effect has been established between the mean load and the amplitude of the system response. The dynamic behavior of the nonlinear Hill's equation has been compared to the NLTI case and the differences in response have been highlighted. Further, a

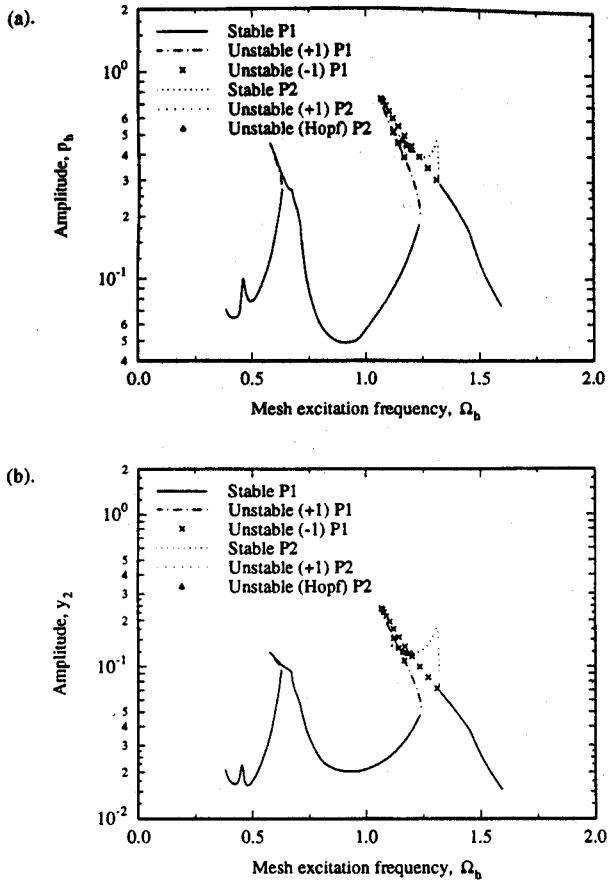

FIG. 14. Simulation results for Munro's rig[17] for design load conditions with (a) dynamic transmission error, p_h, and (b) bearing displacement, y_2; see Table I for parameters used.

geared system has been analyzed as an application of the nonlinear Hill's equation. The prior model of Kahraman and Singh[18] has been reexamined to provide improved correlation with prior experimental data. Also, new interpretation for some of the nonlinear phenomena in the experimental data has been provided.

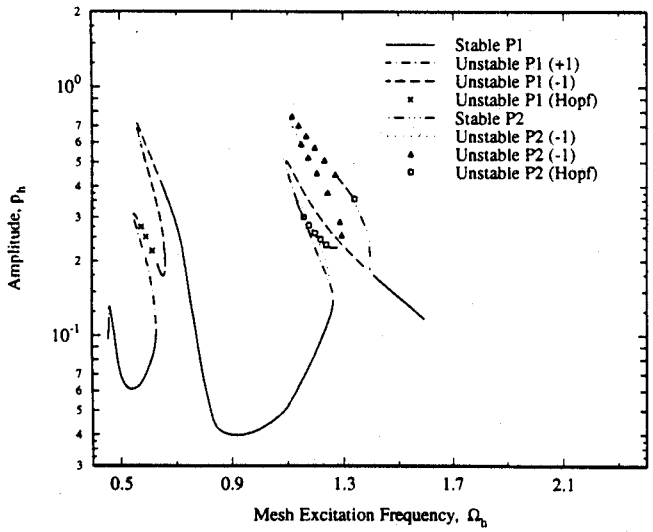

FIG. 15. Simulation results of dynamic transmission error, p_h, for Munro's rig[17] for half-design load conditions.

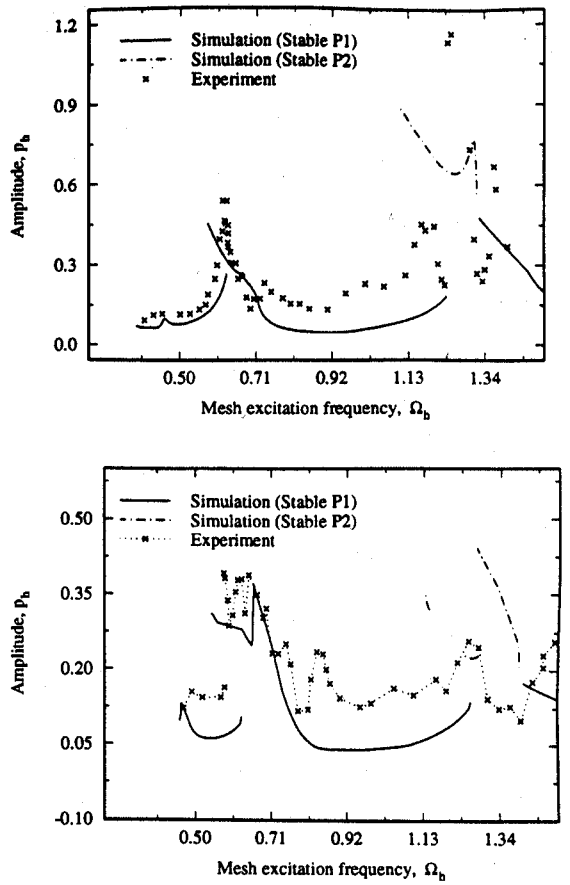

FIG. 16. Comparison of simulation and experimental results for Munro's rig:[17] (a) design load and (b) half-design load; see Table I for parameters used.

ACKNOWLEDGMENTS

The authors would like to thank the U.S. Army Research Office (URI Grant No. DAAL-03-92-G-0120; Project Monitor Dr. T. L. Doligalski) for supporting this research. We also wish to acknowledge Dr. Todd Rook and Dr. Harsh Vinayak for the valuable discussions during the course of this research.

[1] J. P. Den Hartog, *Mechanical Vibrations* (McGraw-Hill, New York, 1940).
[2] N. W. McLachlan, *Theory and Application of Mathieu Functions* (Clarendon, Oxford, 1947).
[3] A. Tondl, *Some Problems in Rotor Dynamics* (Czechoslovakian Academy of Sciences, Prague, 1965).
[4] J. A. Richards, *Analysis of Periodically Time-Varying Systems* (Springer-Verlag, New York, 1983).
[5] A. H. Nayfeh and D. T. Mook, *Nonlinear Oscillations* (Wiley, New York, 1979).
[6] C. S. Hsu and W.-H. Cheng, "Applications of the Theory of Impulsive Parametric Excitation and New Treatments of General Parametric Excitation Problems," J. Appl. Mech. **40**, 78–86 (1973).
[7] C. S. Hsu and W.-H. Cheng, "Steady State Response of a Dynamical System under Combined Parametric and Forcing Excitation," J. Appl. Mech. **41**, 371–378 (1973).
[8] H. Troger and C. S. Hsu, "Response of a Non-linear System under Combined Parametric and Forcing Excitation," J. Appl. Mech. **44**, 179–181 (1977).
[9] N. Haquang, D. T. Mook, and R. H. Plaut, "Non-linear Analysis of the Interactions between Parametric and External Excitations," J. Sound Vib. **118**, 425–439 (1987).

[10]R. I. Zadoks and A. Midha, "Parametric Stability of a Two-Degree-of-Freedom Machine System: Part I—Equations of Motion and Stability," J. Mechanisms, Transmissions Automation Des. **109**, 210–215 (1987).
[11]F. H. Ling and X. X. Wu, "Fast Galerkin Method and its Application to Determine Periodic Solutions of Non-Linear Oscillators," Int. J. Nonlinear Mech. **22**, 89–98 (1987).
[12]R. Seydel, *From Equilibrium to Chaos: Practical Bifurcation and Stability Analysis* (Elsevier, New York, 1988).
[13]C. Padmanabhan and R. Singh, "Analysis of Periodically Excited Non-Linear Systems By a Parametric Continuation Technique," J. Sound Vib. **184**, 35–58 (1995).
[14]C. Padmanabhan and R. Singh, "Dynamics of a Piecewise Non-Linear System Subject to Dual Harmonic Excitation Using Parametric Continuation," J. Sound Vib. **184**, 767–799 (1995).
[15]H. N. Özgüven and D. R. Houser, "Mathematical models used in Gear Dynamics—A Review," J. Sound Vib. **121**, 383–411 (1988).
[16]M. Hortel, "Forced Damped Vibration in a Non-linear Parametric System of Gears with several degrees-of-freedom," Proceedings of the 4th Conference on Non-linear Oscillations, Prague, Czechoslavakia, 1968, pp. 337–346.
[17]R. G. Munro, "The Dynamic Behavior of Spur Gears," Ph.D. dissertation, University of Cambridge, 1962.
[18]F. Kücükay, "Dynamic Behavior of High Speed Gears," Proceedings Third International Conference on Vibrations in Rotating Machinery, Yorkshire, England, 1984, Paper C317/84, pp. 81–90.
[19]A. Kahraman and R. Singh, "Interactions between Time-Varying Mesh Stiffness and Clearance Non-linearities," J. Sound Vib. **146**, 135–156 (1991).
[20]A. Kubo, "Stress Condition, Vibrational Exciting Force, and Contact Pattern of Helical Gears with Manufacturing and Alignment Errors," J. Mech. Des. **100**, 77–84 (1978).